Symmetry-breaking instability of quadratic soliton bound states

Michaël Delqué,[1,2] Gil Fanjoux,[2] Hervé Maillotte,[2] Pascal Kockaert,[1] Thibaut Sylvestre,[2] and Marc Haelterman[1,*]

[1]*Service OPERA-photonique, CP194/5, Université Libre de Bruxelles U.L.B. Avenue F.D. Roosevelt, B-1050 Bruxelles, Belgium*

[2]*Département d'Optique P.M. Duffieux, Institut FEMTO-ST, Université de Franche-Comté, CNRS UMR 6174, F-25030 Besançon, France*

(Received 19 November 2010; published 7 January 2011; publisher error corrected 13 January 2011)

We study both numerically and experimentally two-dimensional soliton bound states in quadratic media and demonstrate their symmetry-breaking instability. The experiment is performed in a potassium titanyl phosphate crystal in a type-II configuration. The bound state is generated by the copropagation of the antisymmetric fundamental beam locked in phase with the symmetrical second harmonic one. Experimental results are in good agreement with numerical simulations of the nonlinear wave equations.

DOI: 10.1103/PhysRevA.83.013807 PACS number(s): 42.65.Tg, 42.65.Ky

I. INTRODUCTION

Since the early works of Torruellas *et al.* [1], Torner *et al.* [2,3], and Boardman *et al.* [4], it has been well known that second-order nonlinearity ($\chi^{(2)}$) can lead to efficient self-guiding effects. In that context, soliton beam propagation in nonlinear media commonly used for frequency conversion has been observed in plenty of configurations (see Ref. [5] for a review) including, in particular, the $(2+1)$-dimensional [$(2+1)$D] geometry [1,3,6] for which Kerr solitons are not stable [7]. As expected in a medium that supports soliton propagation, modulation instability (MI) [8] has also been observed in quadratic materials [9–12]. In a theoretical paper, Haelterman *et al.* predicted the existence in these media of multiple soliton bound states analogous to those of Kerr media [13]. In Kerr media these bound states have a vector nature in the sense that they consist of coupled linearly polarized solitons of orthogonal polarization in phase quadrature [14]. In quadratic media the bound states are the result of the coupling of two parallel quadratic soliton beams of the same polarization but having π-out-of-phase fundamental field envelopes. It was shown in Ref. [13] that these quadratic bound states exhibit a symmetry-breaking instability that results in a power transfer from one soliton of the bound state to the other, in a way similar to what happens in Kerr soliton bound states. The existence and the symmetry-breaking instability of the soliton bound states have already been demonstrated in Kerr media [15,16]. Until now, no experimental demonstrations have been presented concerning the existence and the propagation dynamics of quadratic bound soliton states whereas collisions between individual solitons [17] have been observed [18]. This can be explained by the difficulty in performing the polarization and spatial shaping of the bound-state components while assuring the appropriate phase relation between them. In the Kerr configuration only, the phase-locking problem can be bypassed by using circularly polarized components. Here, we overcome this issue by using a couple of phase plates controlling the spatial features of the beams and their phase relation and demonstrate the quadratic bound-state dynamics.

In the present paper, we provide a detailed study of the dynamical features of quadratic soliton bound states. In particular, we demonstrate experimentally that the bound states undergo the theoretically predicted symmetry-breaking instability. However, for practical reasons we considered in our experiment the generation and propagation of the bound states in a $(2+1)$D geometry whereas theory has been developed for the $(1+1)$D geometry [13]. In addition, we considered a type-II phase-matching configuration that implies walk-offs between the waves involved in the underlying three-wave-mixing process. For these reasons we first had to check the existence of the bound states with two transverse dimensions in the type-II phase-matching arrangement. This was done numerically on the basis of a realistic wave propagation model. We first calculated the stationary soliton solutions of this model by means of a standard relaxation method. This calculation allowed us to confirm the existence of $(2+1)$D quadratic soliton bound states in a type-II phase-matching configuration. We then simulated the propagation of these bound states to confirm their invariant nature as well as to show that they suffer a symmetry-breaking instability exactly as predicted in Ref. [13] for the $(1+1)$D geometry. Finally, we provide a statistical analysis from laser shots of the symmetry-breaking instability of the bound states.

II. NUMERICAL STUDY

As in the first demonstration of the existence of the quadratic soliton [1], we chose the commonly used potassium titanyl phosphate (KTP) crystal as nonlinear quadratic material. The reasons for this choice are its availability in large format (centimeter size), its high efficiency, and its high damage threshold (>500 MW/cm^2 [19]).

In KTP the propagation of the fundamental and second harmonic fields in the type-II phase-matching configuration can be described by a set of three equations [1]. They model the propagation of the three fields involved in the nonlinear wave coupling, i.e., ordinary and extraordinary polarized fundamental fields (FF) and the extraordinary polarized second harmonic field (SH):

$$\begin{cases} i\frac{\partial U_o}{\partial z} + \frac{1}{2k_o^{\mathrm{FF}}}\Delta U_o + \frac{\gamma}{n_o^{\mathrm{FF}}} V_e U_e^{\star} = 0, \\ i\frac{\partial U_e}{\partial z} + \frac{1}{2k_e^{\mathrm{FF}}}\Delta U_e - i\rho_{e,x}^{\mathrm{FF}}\frac{\partial U_e}{\partial x} - \delta_1 U_e + \frac{\gamma}{n_e^{\mathrm{FF}}} V_e U_o^{\star} = 0, \\ i\frac{\partial V_e}{\partial z} + \frac{1}{2k_e^{\mathrm{SH}}}\Delta V_e - i\rho_{e,x}^{\mathrm{SH}}\frac{\partial V_e}{\partial x} - \delta_2 V_e + 2\frac{\gamma}{n_e^{\mathrm{SH}}} U_o U_e = 0, \end{cases} \quad (1)$$

with U_o, U_e, and V_e the ordinary, extraordinary FF, and extraordinary SH, and n_o^{FF}, n_e^{FF}, and n_e^{SH} their refractive

*mhaelter@ulb.ac.be

indices, respectively. Δ stands for the 2D transverse Laplacian operator $\frac{\partial^2}{\partial x^2} + \frac{\partial^2}{\partial y^2}$, and $\rho_{e,x}^{\mathrm{FF}} = 0.19^\circ$ and $\rho_{e,x}^{\mathrm{SH}} = 0.28^\circ$ are the spatial walk-off angles of the two extraordinary beams. We assume that the KTP crystal is cut for second harmonic generation at 1064 nm. This implies the angle values $\theta = 90^\circ$ (corresponding to propagation in the X-Y crystal plane), $\phi = 23.5^\circ$ (with $\tan\phi = Y_0/X_0$; $\overrightarrow{(X_0, Y_0)}$ defining the beam propagation direction in the X-Y crystal plane). Note that the coordinates axes (x,y,z) are chosen so that the x axis is in the direction of the walk-off. The parameters δ_1 and δ_2 are the phase mismatches between the two FF fields and the SH field. The nonlinear coefficient is written as $\gamma = d_{\mathrm{eff}}\omega_{\mathrm{FF}}/c$, where ω_{FF} is the FF angular frequency, c is the speed of light in vacuum, and d_{eff} is the effective nonlinearity given by $d_{\mathrm{eff}} = d_{31}\sin^2\phi + d_{24}\cos^2\phi^2$ (for $\theta = 90^\circ$), with $d_{31} = 1.95$ pm/V and $d_{24} = 3.9$ pm/V [19].

Compared to the model of Ref. [13] in which the quadratic soliton bound states and their instability have been predicted, the main differences are the 2D transverse geometry and the type-II phase-matching configuration (two FF components leading to a system of three coupled equations instead of two) with the associated spatial walk-off between the three field components. Given these fundamental differences, we have first checked numerically the existence of the bound states as stationary solutions of Eqs. (1) and then we studied numerically their stability through a standard beam propagation method. These preliminary studies are the object of the following paragraphs.

A. Soliton bound states

The stationary solutions of the model (1) have been calculated numerically using the so-called relaxation method [20], Sec. 17.3]. We considered as initial guess a two-lobe structure with antisymmetric profiles in the FF components and a symmetric profile in the SH component so as to mimic the $(1+1)$D soliton solution of Ref. [13]. The two lobes are naturally centered on the y axis, so that the system symmetry is not broken by the walk-offs that are in the x direction.

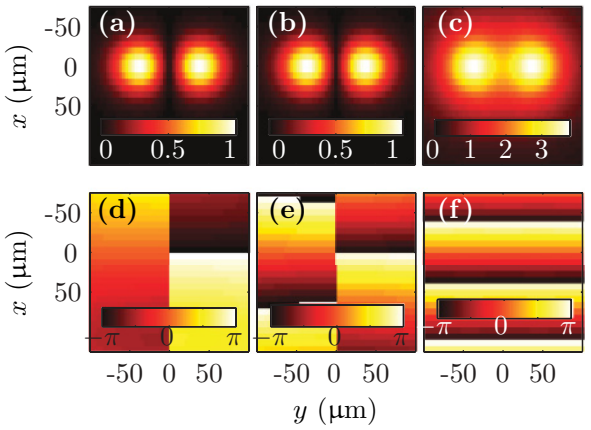

FIG. 1. (Color online) Quadratic soliton bound state corresponding to a total power of 29 kW as calculated numerically from Eqs. (1) with the experimental parameters given in the text. Shown are amplitude profiles of (a) U_o, (b) U_e, and (c) V_e and their corresponding phase profiles [(d), (e), and (f), respectively].

An example of a calculated quadratic soliton bound state is depicted in Fig. 1. One can clearly see that each component exhibits a dual-hump structure and a phase slope in the walk-off direction. The FFs carry a π phase step at $y = 0$, their profiles being antisymmetric in the y direction, in contrast to SH one, which is symmetric. The bound state can then be described as a couple of quadratic solitons (the left and right intensity lobes) propagating invariantly side by side owing to the interaction equilibrium ensured by the π phase relation between their fundamental components. In the following, the bound-state dynamics will be described by means of the left and right soliton behaviors.

This solution has been computed for a crystal misalignment of -0.32° with respect to the phase-matching angle of $\phi = 23.5^\circ$. This misalignment corresponds to a phase mismatch $\delta_k = \omega_{\mathrm{FF}}/c(n_o^{\mathrm{FF}} + n_e^{\mathrm{FF}} - 2n_e^{\mathrm{SH}}) < 0$. This negative phase mismatch is required for the existence of soliton bound states [13] although quadratic solitons exist under both positive and negative phase-mismatch condition [5].

B. Symmetry-breaking dynamics

Solving Eqs. (1) by means of a $(2+1)$D split-step Fourier method we simulated the propagation of these quadratic soliton bound states. These simulations will provide more information on the physics of the soliton bound states as they give access to the amplitude and phase evolution during their propagation and their dependency on the perturbation. The output profiles of the three interacting waves U_o, U_e, and V_e, are presented in Fig. 2. As expected, Figs. 2(a1)–2(a3) show that the soliton bound state propagates undistorted;

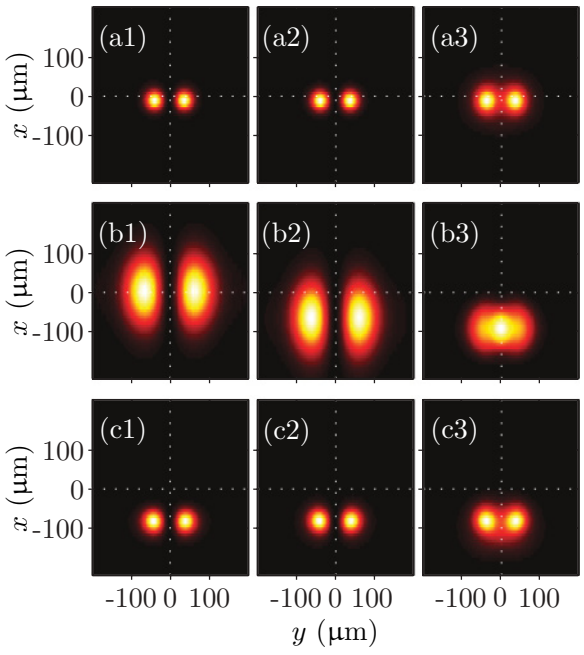

FIG. 2. (Color online) Simulated output intensity profiles of the three interacting waves after 2 cm of propagation of (a) the numerical bound-state solution of Fig. 1; (b) the same initial conditions as in (a) but in the linear regime (low power) and in the absence of initial phase slope in the x direction; (c) the same as in (b) but at soliton power.

in particular, it conserves its profile and, in spite of the walk-offs, its propagation direction (with the total power here being 29 kW). The absence of visible walk-off is naturally due to the compensation of the initial phase slopes in the input profiles. Note that the compensation is not perfect as a slight (≈10-μm) translation in the direction of the walk-off is observable in Figs. 2(a1)–2(a3). This can be explained by the limited transverse resolution of our numerical simulations (8 and 4 μm in the x and y directions, respectively) as imposed by computational limitations. However, the remaining drift is far lower than what can be observed without phase slope compensation, as described thereafter.

Figures 2(b1)–2(b3) show the output intensity profiles of the same soliton bound-state envelopes but in the linear regime of propagation, that is, at very low power (the total power here being 29 W) and in the absence of the walk-off compensation phase slopes. The observed beam broadening clearly shows that diffraction governs propagation. We also see that the walk-off separates the different beam components: −62- and −94-μm x translation for the extraordinary FF and SH, respectively, as expected from the values of the two walk-off angles in Eqs. (1).

Figures 2(c1)–2(c3) present the propagation of the same input envelopes without phase slope, but with the appropriate power corresponding to the soliton bound-state solution computed numerically and shown in Fig. 1. It is clear from this result that the quadratic nonlinearity induces spatial self- and mutual trapping of the field components even in the absence of phase slope in the initial field profiles. The walk-off only results in a tilted propagation in the x direction. A common translation of −82 μm in x is observed on each beam. This result is of importance because it demonstrates that soliton propagation does not require an initial phase slope in the beam profiles. The absence of phase slope is only responsible for a drift while the self- and mutual confinement is preserved. In our experiment it is therefore legitimate and convenient to generate the beam profiles without their phase slope, which strongly simplifies the beam-shaping setup.

Propagation simulations of field profiles as obtained in the experiment were performed to observe the generation dynamics of the bound state starting from nonideal profiles and to check the stability of the soliton bound states. The SH profile is a simple circular Gaussian beam while the FF profiles are formed by juxtaposing two out-of-phase circular Gaussian beams of smaller diameter. For the three beams the phase profile is flat. A 10% intensity noise with a random phase has been added to the three envelopes in order to mimic experimental conditions. Figure 3 presents a typical result of the simulations with a total beam power of 20 kW. The input beams are shown in Fig. 3(a). The other figures allow us to identify three steps in the propagation dynamics. Over the first 5 mm we see that the SH beam is spontaneously reshaped to adopt the two-hump profile of the exact soliton bound-state solution [Fig. 3(b)]. After 2 cm the FF envelopes start to exhibit an asymmetry [Fig. 3(c)], which is the signature of the symmetry-breaking instability predicted in the (1 + 1)D geometry in Ref. [13]. The instability develops rapidly and results in an almost complete transfer of power from one soliton of the bound state to the other, exactly as what happens in the Kerr-type soliton bound state [21] [Fig. 3(d)]. At this stage the beams progressively adopt the profiles of the well-known stable single quadratic soliton. As the symmetry-breaking instability is induced by noise, the direction of the energy transfer from one lobe to the other is random. As a result, we can expect in the experiment to observe from shot to shot a random left-right symmetry breaking of the laser beam.

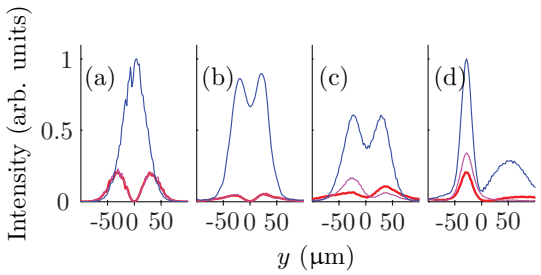

FIG. 3. (Color online) Simulated intensity profiles in the y direction (resulting from integration in x) of the beams corresponding to a total power of 20 kW. The red (bottom bold), magenta (bottom), and blue (upper) lines represent U_o, U_e, and V_e, respectively. (a) Input $z = 0$ cm, (b) $z = 0.5$ cm, (c) $z = 2$ cm, and (d) $z = 5$ cm.

III. EXPERIMENTAL SETUP

The experimental setup is depicted in Fig. 4. A Nd:YAG Q-switched mode-locked laser emitting 1064-nm, 55-ps pulses with energy in the millijoule range is used to generate both the FF and the SH fields. After cleaning up the beam profile through spatial filtering, the linear polarization is set to 45° by using a half-wave plate combined with a polarizer so as to reach the maximum SH generation efficiency (≈50%) in a 2-cm-long KTP crystal cut for type-II phase matching (KTP1). The FF and SH beams are then shaped in a cylindrical lens arrangement (L_x,L_y) and launched into the second KTP crystal (KTP2, with the same specifications as KTP1).

The phase profiles of the beams are shaped after the lenses by means of two glass plates P_1 and P_2. P_1 is a nonparallel plate (truncated prism) with an angle of 1° between its main faces. A simple translation of this plate in the transverse plane allows for a fine tuning of the phase difference between the FF and SH input fields. Experimental results show that a 1-cm translation corresponds approximately to a 2π relative phase shift. Note that this plate induces a spatial misalignment of

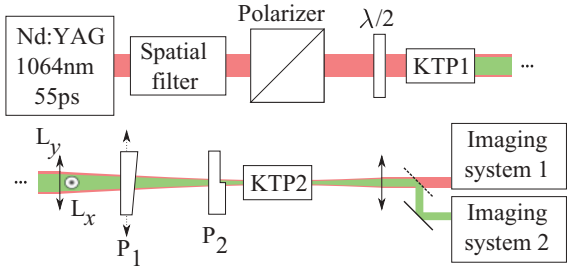

FIG. 4. (Color online) Experimental setup. $\lambda/2$ stands for the half-wave plate. L_x and L_y are cylindrical lenses with focal length of 150 mm in the x direction and 80 mm in the y directions, respectively. P_1 and P_2 are the phase plates. FF and SH are imaged using distinct imaging systems with synchronized CCD cameras.

the FF and SH beams due to dispersion (refraction through a prism); however, the 1° angular aperture is sufficiently small to induce only negligible misalignments. The second plate P_2 is covered on half the surface by a thin glass layer. The layer has a thickness inducing a π phase shift across the FF beam and a nearly 2π phase shift across the SH beam. Due to diffraction the π phase shift in the FF beam induces in the focal plane of the lenses two well-separated lobes of opposite phase while the perturbation caused by the nearly 2π phase shift in the SH beam is merely washed out provided that this phase jump is established on a sufficiently short distance in the transverse plane. One can therefore reasonably admit that this shaping process leads to field distributions that are close to those of the theoretical soliton bound state.

In a first step, only the KTP1 crystal is placed in the beam and oriented by means of a couple of rotation stages in order to optimize frequency conversion. According to numerical simulation a conversion of 90% would be necessary but, due to experimental constraints (available power and crystal length), a maximum conversion of 50% has been achieved. This limit is not critical as the excess FF energy is lost in the crystal KTP2 through radiative waves in the soliton generation process. The KTP2 crystal is then placed in the focal plane of the lenses. KTP2 is aligned by generating first a fundamental (single-hump) quadratic soliton. It is then misaligned by a few tenths of degrees with respect to the phase-matching angle in order to get the negative phase mismatch necessary for the generation of soliton beams. The generation of a fundamental (single-hump) quadratic soliton is obtained through the introduction of phase plate P_1 by finely tuning its transverse position in the beam. Then the phase plate P_2 is introduced to induce the π phase shift in the middle of the FF beam. The setup is therefore ready to study through power tuning the formation and the stability of the two-hump quadratic soliton bound state. The power was adjusted by using a set of absorptive density filters to obtain the most polarization- and wavelength-insensitive power tuning.

As the KTP2 crystal is only 2 cm long, the symmetry breaking of the beam can only be observed at the first stage of its development, as illustrated by the simulated output profiles of Fig. 3(c). The fully developed left-right symmetry breaking leading to complete energy transfer, as illustrated in Fig. 3(d), would require a 5-cm-long crystal.

IV. EXPERIMENTAL RESULTS

A. Two-dimensional profiles

Our results are presented in Fig. 5. Figures 5(a1)–5(a3) show the input intensity profiles of the three fields U_o, U_e, and V_e, respectively. This allows us to check the efficiency of the beam-shaping technique. As can be seen, a rather smooth and symmetric dual-lobe structure is obtained in both FF components, while the SH field exhibits a single-lobe profile. The visible distortion of this profile is attributed to the effect of the finite-width SH 2π phase shift induced by the shaping setup. Note however that what is important is that the SH energy is located in one single lobe well centered on the phase defect of the FF fields.

The output profiles at low power are presented in Figs. 5(b1)–5(b3). As expected, the three components undergo

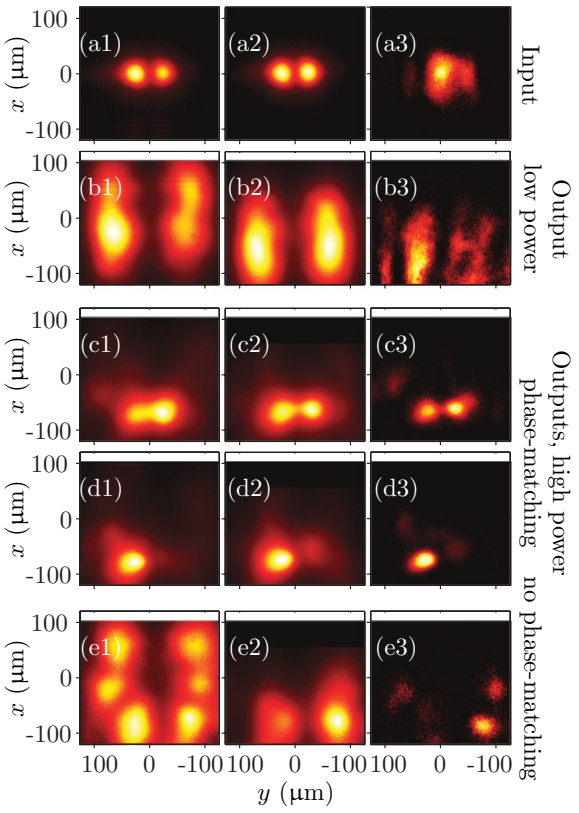

FIG. 5. (Color online) Experimental intensity profiles of U_o, U_e, and V_e in the first, second, and third column, respectively. (a) Input condition, (b) output in the low-power regime, (c,d) output at soliton power ≈ 60 kW showing both the soliton bound state and its symmetry breaking, and (e) output at soliton power but with an unfavorable FF and SH phase relation.

a strong diffraction and a clear spatial separation due to the birefringence walk-off in the crystal. Note that in the present case propagation is not strictly linear, as SHG clearly occurs from the diffracted FF beam wings, which results in the distorted FF profiles and SH intensity background of Fig. 5(b). One can estimate that the FF extraordinary and SH fields undergo ≈ −55- and ≈ −100-μm walk-of-induced x translations. These values are in good agreement with those predicted by the numerical simulation of Fig. 2(b).

Figures 5(c1)–5(c3) show the three output beams obtained at a power of ≈60 kW for which self-guiding is observed. As can be seen, the FF and SH beams are now nicely self-guided through mutual trapping. Their nonlinear interactions compensate not only for diffraction but also for the difference in walk-off angles between the field components. The walk-off is now clearly the same for the three components, resulting in a final translation of approximately 68 μm. Moreover, the SH intensity distribution [Fig. 5(c3)] exhibits a fine dual-lobe structure which reflects the nonlinear beam-reshaping process numerically predicted and illustrated in Fig. 3. This observation clearly demonstrates the existence of the two-hump quadratic soliton bound state theoretically predicted in Ref. [13].

However, this result is not obtained systematically. The experiment is repeated and from one laser shot to another there are significant dissimilarities. In most cases the intensity

profiles adopt a one-lobe structure randomly displaced either to the left or the right with respect to the center of the above symmetrical profile. This behavior is a clear signature of the symmetry-breaking instability.

A typical example of a symmetry-broken beam is shown in Figs. 5(d1)–5(d3) for exactly the same experimental conditions as those of Figs. 5(c1)–5(c3). As can be seen, the three initially symmetric fields have transferred almost all their power to a single-lobe structure displaced to the left of the initial beam axis. Quite remarkably, the resulting beam is quite smooth and well confined, which shows that the compensation of diffraction and the mutual field trapping are both maintained in the symmetry-breaking process. This is in excellent agreement with the numerical simulations that show in the final stage of the instability process the formation of a single-lobe fundamental quadratic soliton.

Figures 5(e1)–5(e3) show what is observed when the relative phase between the FF and SH fields is not controlled (phase plate P_1 is removed from the setup). Even at power levels corresponding to the soliton regime (≈60 kW), diffraction is no longer compensated and the mutual field trapping is reduced to the formation of some randomly distributed spots. It is the contrast between this erratic behavior and the soliton regime that allowed us to finely tune the relative phase between the FF and SH fields by means of the phase plate P_1.

B. Statistical study

Figure 6 shows the result of a statistical study of the instability. It shows histograms of a measure of the beam asymmetry. Because of the radiative wave and noise background in the beam images (mainly due to the absence of diffraction compensation in the pulse wings), the beam asymmetry could not be evaluated simply through the first-order intensity distribution moment. We adopted an alternative technique that consisted in making a fit of the two beam peaks by means of two separate and independent Gaussian functions (the two-dimensional intensity distribution being first integrated over the x direction so that the fit is performed on the two-peak intensity profile in y). We then defined the beam asymmetry parameter S as being the ratio between the intensity of the left beam Gaussian fit and the overall beam intensity. The parameter S is then the relative weight of the left beam, a value of 0.5 corresponding to a symmetric beam.

Figure 6(a) shows the S distribution of the input beam. As can be seen, the input beam is not perfectly stable due to variations of the spatial profile of the Q-switched laser pulses from shot to shot (since there are 10% intensity fluctuations in the spatial profiles of the laser pulses).

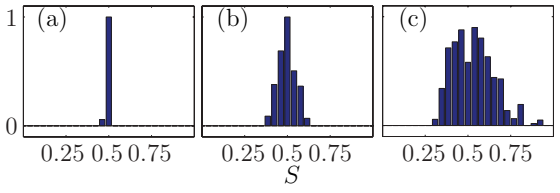

FIG. 6. (Color online) Statistical study of the soliton symmetry-breaking process: (a) input beam, 66 laser shots; (b) output in the low-power regime, 87 laser shots; (c) output in the soliton regime, 159 shots.

Figure 6(b) shows the statistics for the output beam at the relatively low power (≈1 kW) corresponding to Fig. 5(b1)–5(b3). As previously mentioned, at this power there is non-negligible energy transfer between the FF and SH components, leading to some complexity. The resulting distribution width reveals that nonlinear effects already induce some kind of instability. However, the distribution remains peaked at the origin, showing that the symmetric output is still the most probable.

Figure 6(c) reveals that in the soliton regime (60 kW) the distribution is split into two main lobes of approximately the same height. Clearly the probability of getting a symmetric event becomes much weaker and in a large majority of the events symmetry breaking occurs. The large width of the distribution lobes shows that the fundamental quadratic soliton beam resulting from the symmetry breaking has an orientation that greatly fluctuates from shot to shot.

V. CONCLUSION

In summary, we have shown numerically and experimentally the existence of the $(2+1)$D quadratic soliton bound state as a stationary solution of the full nonlinear wave propagation model including birefringence walk-off. The experiments were performed by launching in a type-II KTP crystal a field configuration that is as close as possible to the theoretical soliton-bound-state solution, which means that we controlled the relative phase between the fundamental and second harmonic fields and that we shaped the fundamental field into an antisymmetric two-lobe amplitude profile. Although the propagation length is relatively short (2 cm), the symmetry-breaking instability of the soliton bound state has been clearly observed thanks to the pulse-to-pulse noise fluctuations of the Q-switched laser used for the experiment. From shot to shot the spatial profile changes sufficiently to get two regimes of propagation in the same experiment. Depending to the shot, the noise perturbation spatial asymmetry is either weak enough to allow for steady propagation of the bound state or, conversely, able to seed the instability, in which case the symmetry breaking leads to a single-lobe fundamental quadratic soliton walking transversely at variable angles. We provided a statistical study that shows the robustness of the symmetry-breaking dynamics that is at play in the quadratic soliton bound state, a feature that might have some potential application for all-optical signal processing in which beam self-guiding and switching processes are key functions.

ACKNOWLEDGMENTS

This work is supported by the Interuniversity Attraction Pole program of the Belgian government under Grant No. IAP6-10 and by a ULB fellowship. This work benefits from the Programme International de Coopération Scientifique PICS-3742 of the French Centre National de la Recherche Scientifique (CNRS). A part of this work was supported by the Groupement de Recherche Photonique Nonlinéaire et Milieux Microstructurés GDR-3073 created by CNRS. Computations have been done on the Mesocentre de calcul de Franche-Comté machine.

[1] W. E. Torruellas, Z. Wang, D. J. Hagan, E. W. Van Stryland, G. I. Stegeman, L. Torner, and C. R. Menyuk, Phys. Rev. Lett. **74**, 5036 (1995).
[2] L. Torner, C. R. Menyuk, and G. I. Stegeman, Opt. Lett. **19**, 1615 (1994).
[3] L. Torner, C. R. Menyuk, W. E. Torruellas, and G. I. Stegeman, Opt. Lett. **20**, 13 (1995).
[4] A. D. Boardman, K. Xie, and A. Sangarpaul, Phys. Rev. A **52**, 4099 (1995).
[5] A. V. Buryak, P. Di Trapani, D. V. Skryabin, and S. Trillo, Phys. Rep. **370**, 63 (2002).
[6] X. Liu, L. J. Qian, and F. W. Wise, Phys. Rev. Lett. **82**, 4631 (1999).
[7] V. E. Zakharov and A. B. Shabat, Sov. Phys. JETP **34**, 62 (1972).
[8] V. I. Bespalov and V. I. Talanov, JETP Lett. **3**, 307 (1966).
[9] A. D. Boardman, P. Bontemps, and K. Xie, J. Opt. Soc. Am. B **14**, 3119 (1997).
[10] A. De Rossi, S. Trillo, A. V. Buryak, and Y. S. Kivshar, Phys. Rev. E **56**, R4959 (1997).
[11] D.-M. Baboiu and G. I. Stegeman, Opt. Lett. **23**, 31 (1998).
[12] R. Schiek, H. Fang, R. Malendevich, and G. I. Stegeman, Phys. Rev. Lett. **86**, 4528 (2001).
[13] M. Haelterman, S. Trillo, and P. Ferro, Opt. Lett. **22**, 84 (1997).
[14] M. Haelterman, A. P. Sheppard, and A. W. Snyder, Opt. Lett. **18**, 1406 (1993).
[15] C. Cambournac, T. Sylvestre, H. Maillotte, B. Vanderlinden, P. Kockaert, P. Emplit, and M. Haelterman, Phys. Rev. Lett. **89**, 083901 (2002).
[16] M. Delqué, M. Chauvet, H. Maillotte, and T. Sylvestre, Opt. Commun. **249**, 285 (2005).
[17] Y. Baek, R. Schiek, G. I. Stegeman, I. Baumann, and W. Sohler, Opt. Lett. **22**, 1550 (1997).
[18] B. Costantini, C. De Angelis, A. Barthelemy, B. Bourliaguet, and V. Kermene, Opt. Lett. **23**, 424 (1998).
[19] Our crystals are provided by EKSMA optics. See [http://www.eksmaoptics.com] for more information.
[20] W. H. Press, S. A. Teukolsky, W. T. Vetterling, and B. P. Flannery, *Numerical Recipes in C: The Art of Scientific Computing*, 2nd ed. (Cambridge University Press, Cambridge, 1992).
[21] P. Kockaert and M. Haelterman, J. Opt. Soc. Am. B **16**, 732 (1999).